Inorganic Chemistry

Article

pubs.acs.org/IC

Sky-Blue Luminescent Au^I–Ag^I Alkynyl-Phosphine Clusters

Igor O. Koshevoy,*[,†] Antti J. Karttunen,[†,‡] Ilya S. Kritchenkou,[§] Dmitrii V. Krupenya,[§] Stanislav I. Selivanov,[§] Alexei S. Melnikov,[∥] Sergey P. Tunik,*[,§] Matti Haukka,[†,‡] and Tapani A. Pakkanen[†]

[†]Department of Chemistry, University of Eastern Finland, Joensuu 80101, Finland

[‡]Department of Chemistry, University of Jyväskylä, 40014 Jyväskylä, Finland

[§]Department of Chemistry, St. Petersburg State University, Universitetskii pr. 26, 198504, St. Petersburg, Russia

[∥]Department of Physics, St. Petersburg State University, Ulijanovskaja 3, 198504, St. Petersburg, Russia

Supporting Information

ABSTRACT: Treatment of the $(AuC_2R)_n$ acetylides with phosphine ligand 1,4-bis(diphenylphosphino)butane (PbuP) and Ag^+ ions results in self-assembly of the heterobimetallic clusters of three structural types depending on the nature of the alkynyl group. The hexadecanuclear complex $[Au_{12}Ag_4(C_2R)_{12}(PbuP)_6]^{4+}$ (**1**) is formed for R = Ph, and the octanuclear species $[Au_6Ag_2(C_2R)_6(PbuP)_3]^{2+}$ adopting two structural arrangements in the solid state were found for the aliphatic alkynes (R = Bu^t (**2**), 2-propanolyl (**3**), 1-cyclohexanolyl (**4**), diphenylmethanolyl (**5**), 2-borneolyl (**6**)). The structures of the compounds **1**–**4** and **6** were determined by single crystal X-ray diffraction analysis. The NMR spectroscopic studies revealed complicated dynamic behavior of **1**–**3** in solution. In particular, complexes **2** and **3** undergo reversible transformation, which involves slow interconversion of two isomeric forms. The luminescence behavior of the titled clusters has been studied. All the compounds exhibit efficient sky-blue room-temperature phosphorescence both in solution and in the solid state with maximum quantum yield of 76%. The theoretical DFT calculations of the electronic structures demonstrated the difference in photophysical properties of the compounds depending on their structural topology.

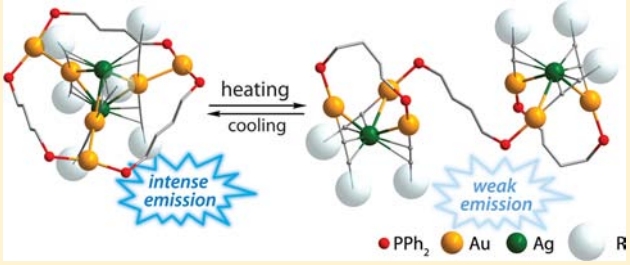

INTRODUCTION

Organometallic complexes of coinage metals represent a fascinating class of coordination compounds, which exhibit a particularly rich chemistry due to the formation of inter- and intramolecular metal–metal bonds (so-called metallophilic interactions) that gives rise to self-assembly of a wide range of homo- and heteronuclear polymetallic species.[1] In addition to this structural diversity and fundamental theoretical interest to the closed-shell metal–metal interactions,[2] the attractive nonlinear optical and photoluminescent properties of these aggregates[3] are the major reasons which determine significant progress of supramolecular chemistry of copper subgroup metal complexes.

The presence of the heterometallic bonds within certain molecular entity often induces very effective photoemission with extremely high quantum yields exceeding 90%.[3b,h,4] The photophysical characteristics of these compounds are strongly dependent on the geometry of the polymetallic core, nature of constituting metals, and electronic properties of the ligand environment. Therefore, understanding the correlations of the structural, stereochemical, and physical properties of these complicated objects is of principle importance for the academic science and also beneficial for the potential optoelectronic applications (e.g., electroluminescent devices, luminescent sensors, and bioimaging labels) through opening a way to predictable and effective tuning of light emission within wide spectral range.

In this respect the alkynyl ligands serve as suitable building blocks due to their ability to coordinate metal ions both in σ- and π-bonding modes thus promoting formation of effective metal–metal contacts. Moreover, the C≡C moieties of these ligands are often involved in charge transfer processes, which occur upon photoexcitation, and therefore can efficiently influence the emission parameters of these complexes.[5] Recent reports from our and other groups on the Au^I–Cu^I heterometallic compounds indicate that weak interactions (e.g., hydrogen bonding) between the noncoordinating groups R of the —C≡C—R ligands have a dramatic effect on the cluster assembly processes and, consequently, on their photophysical properties.[4b,d] It was shown that the use of the hydroxyaliphatic alkynes allows for the preparation of structurally novel complexes showing intense blue phosphorescence. Triplet emission in this spectral region is still rare among gold(I) containing clusters, and such blue luminophores remain a challenge to design and synthesize.[4b,d,6] This prompted us to search for a possibility to prepare complexes showing effective blue luminescence. Taking into account that the Au^I–Ag^I clusters demonstrate a systematic hypsochromic

Received: September 27, 2012
Published: March 21, 2013

   dx.doi.org/10.1021/ic302105a | *Inorg. Chem.* 2013, 52, 3663–3673

Scheme 1. Examples of Au^I–Ag^I Clusters Based on the Diphosphine Ligands

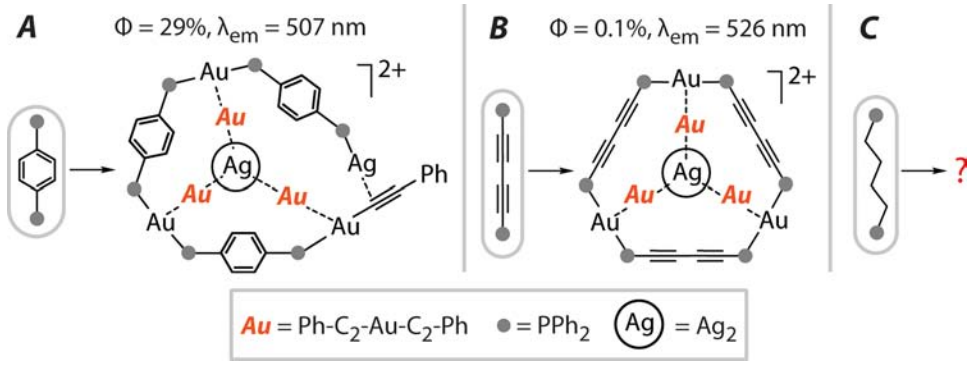

shift of the emission band compared to their Au^I–Cu^I congeners with similar structural motif,[7] we were prompted to focus on the Au^I–Ag^I alkynyl compounds.

The synthesis of the molecular bimetallic alkynyl Cu^I, Ag^I, and Au^I clusters often involve bridging phosphine ligands, which prevent the infinite aggregation and confine the metal core to a certain size and shape.[3h,4c,8] For the preparation of Au^I–Ag^I assemblies in our previous studies we were using rigid 1,4-PPh_2–C_6H_4–PPh_2 and PPh_2–C_2–C_2–PPh_2 diphosphines, which, however, lead to either photodynamically unstable species (Scheme 1 A)[7b,9] or poorly luminescent species (Scheme 1 B),[7c] respectively. Therefore, our intention was to investigate stereochemically flexible diphosphine 1,4-PPh_2–$(CH_2)_4$–PPh_2 as an ancillary ligand to stabilize the polymetallic compounds having different types of alkyne groups (aromatic, aliphatic, hydroxyaliphatic). Moreover, our recent work on the Au^I–Cu^I species bearing 1,4-PPh_2–$(CH_2)_4$–PPh_2 demonstrated that these complexes display a blue-shift of the emission maximum of up to 40 nm in comparison with the structurally analogous compounds based on the 1,4-PPh_2–C_6H_4–PPh_2 ligand without loss of quantum efficiency.[10]

Herein we report on the synthesis of novel Au^I–Ag^I polymetallic aggregates, their structural characterization, and systematic spectroscopic studies of their dynamic behavior in the fluid phase together with the detailed investigation of the photophysical characteristics supported by the theoretical DFT calculations.

EXPERIMENTAL SECTION

General Comments. $(AuC_2R)_n$ complexes (R = Ph, Bu^t, C_3H_7O, $C_6H_{11}O$, $C_{13}H_{11}O$, 1*R*(+)-$C_{10}H_{17}O$) were prepared according to the published procedures.[4d,11] Other reagents and solvents were used as received. The solution ^{1}D, ^{1}H, ^{31}P NMR and ^{1}H–^{1}H COSY spectra were recorded on Bruker Avance 400 and Bruker DPX 300 spectrometers. Mass spectra were measured on a Bruker micrOTOF 10223 instrument in the ESI^+ mode. Microanalyses were carried out in the analytical laboratory of the University of Eastern Finland.

Synthesis of Complexes 1–6. $(AuC_2R)_n$ (0.3 mmol) was suspended in dichloromethane (15 cm^3), and crystalline 1,4-bis(diphenylphosphino)butane (0.155 mmol) was added in one portion. The suspension was stirred for 15 min in the absence of light to give a nearly clear colorless reaction mixture, which was treated with a solution of $AgPF_6$ or $AgClO_4$ (0.1 mmol) in acetone or methanol, respectively (5 cm^3).

$[Au_{12}Ag_4(C_2Ph)_{12}(PPh_2C_4H_8PPh_2)_6](PF_6)_4$ ***(1)***. Yellow-greenish transparent solution was stirred for 24 h, filtered, evaporated, and washed with acetone–hexane mixture (1:1 v/v, 3 × 4 cm^3). Solid residue was recrystallized by gas-phase diffusion of pentane into acetone solution of **1** at +5 °C to give yellow block crystals (74%). ESI MS (*m*/*z*): $[M]^{4+}$ 1640.13 (calcd 1640.17). NMR spectra are not interpretable due to the presence of a dynamic equilibrium of several molecular forms. Anal. Calcd for $Ag_4Au_{12}C_{264}H_{228}F_{24}P_{16}$: C, 44.37; H, 3.22. Found: C, 44.41; H, 3.38.

$[Au_6Ag_2(C_2Bu^t)_6(PPh_2C_4H_8PPh_2)_3](PF_6)_2$ ***(2)***. Colorless solution was stirred for 4 h, filtered, and evaporated. Solid amorphous residue was recrystallized by gas-phase diffusion of pentane into acetone/dichloromethane solution of **2** at +5 °C to give colorless block crystals (89%). ESI MS (*m*/*z*): $[M]^{2+}$ 1580.25 (calcd 1580.27) weak. $^{31}P\{^1H\}$ NMR (CD_3CN, 333 K; *δ*): 35.1 (s, 6 P, minor isomer), 34.2 (s br, major isomer), major/minor 10/1, −144.6 (sept, 2 P, PF_6). ^{1}H NMR (CD_3CN, 333 K; *δ*): major isomer $PPh_2(CH_2)_4PPh_2$ 7.63 (dd, $^3J_{P-H}$ = 11.3, $^3J_{H-H}$ = 7.9 Hz, 24 H, H-ortho), 7.56–7.42 (m, 36 H, H-para H-meta), 2.47 (m br, 12 H, P–CH_2), 1.69 (m br, 12 H, CH_2-CH_2); $\{Au(C_2C(CH_3)_3)_2\}$ 1.35 (s, 54 H, CH_3). Anal. Calcd for $Ag_2Au_6C_{120}H_{138}F_{12}P_8$: C, 41.73; H, 4.03. Found: C, 41.50; H, 4.21.

$[Au_6Ag_2(C_2C_3H_7O)_6(PPh_2C_4H_8PPh_2)_3](ClO_4)_2$ ***(3)***. Yellowish solution was stirred for 4 h, filtered, and evaporated. The amorphous residue was dissolved in methanol (2 cm^3), and colorless microcrystalline precipitate formed within minutes. It was collected and recrystallized by slow evaporation of acetone/dichloromethane/heptane solution at +5 °C to give colorless block crystals (82%). ESI MS (*m*/*z*): $[M]^{2+}$ 1586.17 (calcd 1586.20) weak. $^{31}P\{^1H\}$ NMR (CD_3CN, 283 K; *δ*): 35.5 (s), 33.9 (m br, minor isomer); major/minor 10/3. ^{1}H NMR (CD_3CN, 283 K; *δ*): major isomer $PPh_2(CH_2)_4PPh_2$ 7.68 (m-(ABXX′), $^3J_{P,H}$ = 13, $^3J_{H,H}$ = 7 Hz, 24 H, H-ortho), 7.56 (t, $^3J_{H,H}$ = 7 Hz, 12 H, H-para), 7.48 (dd, $^3J_{H,H}$ = 7 Hz, 24 H, H-meta), 2.90 (m br, 12 H, P–CH_2), ∼2.0 (m br, 12 H, CH_2-CH_2); $\{Au(C_2C(CH_3)_2OH)_2\}$ 4.62 (6H OH), 1.17 (s, 36 H, CH_3). Anal. Calcd for $Ag_2Au_6C_{114}H_{126}Cl_2O_{14}P_6$: C, 40.58; H, 3.76. Found: C, 40.33; H, 3.88.

$[Au_6Ag_2(C_2C_6H_{11}O)_6(PPh_2C_4H_8PPh_2)_3](PF_6)_2$ ***(4)***. Yellow-greenish solution was stirred overnight, filtered, and evaporated. Yellow solid was washed with diethyl ether (2 × 5 cm^3) and recrystallized by gas-phase diffusion of pentane into acetone solution of **4** at +5 °C to give yellow block crystals (93%). ESI MS (*m*/*z*): $[M]^{2+}$ 1706.27 (calcd 1706.30). $^{31}P\{^1H\}$ NMR (CD_3CN, 283 K; *δ*) 35.4 (s, 6 P), −144.6 (sept, $^1J_{P,F}$ = 706 Hz, 2 P; PF_6); (CD_3CN, 323 K; *δ*): 35.4 (s, major isomer), 34.7 (s br, minor isomer), major/minor ∼20/1, −144.6 (sept, 2 P, PF_6). ^{1}H NMR (CD_3CN, 283 K; *δ*): major isomer $PPh_2(CH_2)_4PPh_2$ 7.72 (dm(ABXX′), $^3J_{P,H}$ = 12.5, $^3J_{H,H}$ = 6.3 Hz, 24 H, H-ortho), 7.56 (t, $^3J_{H,H}$ = 7.1 Hz, 12 H, H-para), 7.49 (dd, $^3J_{H,H}$ = 7.1 and 6.3 Hz, 24 H, H-meta), 2.98 (m br, 12 H, P–CH_2), ∼2.2 (m br, 12 H, CH_2-CH_2); $\{Au(C_2C_6H_{10}OH)_2\}$ 4.79 (6H, OH), 1.57 (12H, m br, C_6H_{10}), 1.25 (12H, m br, C_6H_{10}), 1.10 (24H, m br, C_6H_{10}), 0.88 (12H, m br, C_6H_{10});. Anal. Calcd for $Ag_2Au_6C_{132}H_{150}F_{12}O_6P_8$: C, 42.78; H, 4.08. Found: C, 42.63; H, 4.27.

$[Au_6Ag_2(C_2C_{13}H_{11}O)_6(PPh_2C_4H_8PPh_2)_3](ClO_4)_2$ ***(5)***. Yellowish solution was stirred for 4 h, filtered, and evaporated. Yellow solid was washed with diethyl ether (2 × 5 cm^3) and recrystallized by gas-phase diffusion of diethyl ether into dichloromethane/methanol solution of **5** at +5 °C to give pale yellow crystalline material (91%). ESI MS (*m*/*z*): $[M]^{2+}$ 1958.25 (calcd 1958.30). $^{31}P\{^1H\}$ NMR (CD_3CN, 303 K; *δ*): 36.0 (s), 34.7 (m br, minor isomer); major/minor 10/4. ^{1}H NMR (CD_3CN, 303 K; *δ*): major isomer $PPh_2(CH_2)_4PPh_2$ 7.76 (m ABXX′),

dx.doi.org/10.1021/ic302105a | *Inorg. Chem.* 2013, 52, 3663–3673

Table 1. Crystal Data for 1−4 and 6

	1	2	3	4	6
empirical formula	$C_{611}H_{624}Ag_8Au_{24}F_{48}O_{28}P_{32}$	$C_{126}H_{150}Ag_2Au_6F_{12}O_2P_8$	$C_{120}H_{138}Ag_2Au_6Cl_2O_{16}P_6$	$C_{144}H_{176}Ag_2Au_6F_{12}O_{11}P_8$	$C_{658}H_{826}Ag_8Au_{24}Cl_{20}O_{63}P_{24}$
fw	5429.99	3569.76	3490.56	3956.15	16785.63
temp (K)	100(2)	100(2)	100(2)	100(2)	100(2)
λ(Å)	0.710 73	0.710 73	0.710 73	0.710 73	0.710 73
cryst syst	monoclinic	triclinic	triclinic	monoclinic	monoclinic
space group	$C2/c$	$P\bar{1}$	$P\bar{1}$	$P2_1/c$	$P2_1$
a (Å)	39.2864(4)	13.5411(3)	13.1001(5)	26.7717(11)	19.386(3)
b (Å)	32.6616(4)	14.1769(3)	14.0229(6)	28.0375(12)	29.357(5)
c (Å)	27.3632(3)	17.8341(4)	17.8852(8)	21.8698(10)	29.755(5)
α (deg)	90	101.8670(10)	100.807(3)°	90	90
β (deg)	117.1250(10)	99.8630(10)	98.707(2)°	113.6790(10)	90.469(4)
γ (deg)	90	97.3180(10)	98.553(3)	90	90
V (Å^3)	31249.5(6)	3253.66(12)	3136.6(2)	15033.7(11)	16934(5)
Z	2	1	1	4	1
ρ_{calcd} (Mg/m^3)	1.691	1.822	1.848	1.748	1.646
μ(Mo Kα) (mm^{-1})	6.003	7.193	7.471	6.240	5.596
no. reflns.	121 291	50 539	42 284	141 751	189 909
unique reflns.	29073	12791	11663	29495	62540
GOF (F^2)	1.051	1.056	1.029	1.042	1.019
R_{int}	0.0418	0.0237	0.0596	0.0357	0.0362
R1[a] ($I \geq 2\sigma$)	0.0369	0.0243	0.0423	0.0357	0.0357
wR2[b] ($I \geq 2\sigma$)	0.0899	0.0601	0.1039	0.0927	0.0799

[a] $R1 = \Sigma||F_o| - |F_c||/\Sigma|F_o|$. [b] $wR2 = [\Sigma[w(F_o^2 - F_c^2)^2]/\Sigma[w(F_o^2)^2]]^{1/2}$.

$^3J_{P,H}$ = 12.6, $^3J_{H,H}$ = 6.5 Hz, 24 H, H-ortho), 7.62−7.37 (m, 36 H, H-para H-meta), ∼2.2 (m br, 12 H, P−CH_2), 1.73 (m br, 12 H, CH_2-CH_2); {Au(C_2C(C_6H_5)$_2$OH)$_2$} 7.05 (t, $^3J_{H,H}$ = 7.2 Hz, 12 H, H-para), 6.87 (d br, $^3J_{H,H}$ = 6.0 Hz, 24 H, H-ortho), 6.55 (dd, $^3J_{H,H}$ = 7.2 and 6.0 Hz, 24 H, H-meta), 5.79 (s, 6H, OH). Anal. Calcd for $Ag_2Au_6C_{174}H_{150}Cl_2O_{14}P_6$: C, 50.73; H, 3.67. Found: C, 50.66; H, 3.79.

[Au_6Ag_2($C_2C_{10}H_{17}O$)$_6$($PPh_2C_4H_8PPh_2$)$_3$](ClO$_4$)$_2$ (**6**). Yellowish solution was stirred overnight, filtered, and evaporated. Yellow solid was washed with diethyl ether (2 × 5 cm^3) and recrystallized by slow evaporation of its dichloromethane/methanol solution at room temperature to give nearly colorless crystalline material (79%). ESI MS (m/z): $[M]^{2+}$ 1868.40 (calcd 1868.44). $^{31}P\{^1H\}$ NMR (CD_3CN, 283 K; δ): 35.8 (s, major isomer), 36.6 (m br, minor isomer), major/minor 15/2; (CD_3CN, 303 K; δ): 36.4 (s, minor isomer), 35.6 (s br, major isomer), major/minor 10/2. ^1H NMR (CD_3CN, 283 K; δ): major isomer $PPh_2(CH_2)_4PPh_2$ 8.00 (dm(ABXX′), $^3J_{P,H}$ = 12.8, $^3J_{H,H}$ = 6.0 Hz, 12 H, H-ortho), 7.81 (dm(ABXX′), $^3J_{P,H}$ = 12.8, $^3J_{H,H}$ = 6.0 Hz, 12 H, H-ortho), 7.56 (t, $^3J_{H,H}$ = 7.1 Hz, 12 H, H-para), 7.52 (dd, $^3J_{H,H}$ = 7.1 and 6.0 Hz, 24 H, H-meta), 2.97 (m br, 12 H, P−CH_2), 2.25 (m br, 12 H, CH_2-CH_2); {Au($C_2C_{10}H_{16}OH)_2$} 4.36 (s, 6H, O*H*), 3.41 (m br, 6H, $C_{10}H_{16}$), 1.51 (m br, 18H, $C_{10}H_{16}$), 1.13 (m br, 12H, $C_{10}H_{16}$), 0.90 (s, 18H, $C_{10}H_{16}$), 0.76 (s, 18H, $C_{10}H_{16}$), 0.64 (s, 18H, $C_{10}H_{16}$), 0.32 (m br, 6H, $C_{10}H_{16}$). Anal. Calcd for $Ag_2Au_6C_{156}H_{186}Cl_2O_{14}P_6$: C, 47.56; H, 4.76. Found: C, 47.42; H, 4.77.

X-ray Structure Determinations. The crystals of **1**−**4** and **6** were immersed in cryo-oil, mounted in a Nylon loop, and measured at a temperature of 100 K. The X-ray diffraction data were collected on a Bruker Kappa Apex II, Bruker SMART APEX II, or Bruker Kappa Apex II Duo diffractometers using Mo Kα radiation (λ = 0.710 73 Å). The *APEX2*[12] program package was used for cell refinements and data reductions. The structures were solved by direct methods using the *SHELXS-97*[13] programs with the *WinGX*[14] graphical user interface. A semiempirical absorption correction (*SADABS*)[15] was applied to all data. Structural refinements were carried out using *SHELXL-97*.[13] Some of the solvent molecules in the crystals of **1** and **4** were disordered over two sites. Due to partial loss of acetone in **1** and **4** some of these molecules were refined with occupancy of 0.5. One phenylalkynyl group (C9, C10, C37−C42) in **1** together with acetone molecule (C148−C150, O6) were disordered over two sites and were refined with occupancies of 0.63 and 0.37. The aromatic rings were geometrically idealized. Some of the PF_6^- counterions in **1** and **4** were disordered. In **1** (P9, F11−F16) moiety was refined at two equivalent positions with occupancy of 0.5 at each of them. In **4** no suitable disorder model was found for (P8, F7−F12). The P−F and F−F distances for these groups in **1** and **4** were restrained to be equal. The displacement parameters of the atoms F12−F14 (**1**) were restrained so their U_{ij} components approximate to isotropic behavior, while those of the atoms F7−F12 (**2**) were constrained to be equal. One Bu^t group in **2** was disordered over two sites with occupancies of 0.70 and 0.30. Some of the solvent molecules in the crystals of **2** and **6** were omitted as they were disordered and could not been resolved unambiguously. The missing solvent was taken into account by using a *SQUEEZE* routine of *PLATON*.[16] The contribution of the solvent to the cell content was not taken into account. One C_3H_7O group of alkynyl ligand in **3** was disordered. However, no disorder model could be unambiguously built, and geometric restraints were applied. The atoms C7 and O1 of this moiety were restrained so that their U_{ij} components approximate isotropic behavior. In **6** one dichloromethane crystallization molecule was disordered over two sites (C325, Cl9, Cl10 and C425, Cl91, Cl92) and was refined with occupancies 0.45 and 0.55. One of the diethyl ether molecules (C318−C322, O39) was partially lost and refined with occupancy of 0.5. One of the ClO_4^- counterions was disordered between two equivalent positions (Cl4, O25−O28 and Cl41, O35−O38) and was refined with occupancies of 0.59 and 0.41. The Cl−O and O−O distances were restrained to be equal. The displacement parameters of the atoms Cl4, O25−O28 were restrained so their U_{ij} components approximate isotropic behavior. Two phenyl rings of the diphosphine ligands were disordered over two sites each (C79−C84 and C479−C484; C253−258 and C453−C458) and were refined with occupancies of 0.65/0.35 and 0.44/0.55, respectively. The components C478−C484 and C453−C458 of these aromatic rings were geometrically idealized. No disorder model was found for the phenyl rings C229−C234 and C247−C252, which were restrained to make them planar. A series of displacement constraints were applied to these groups. All hydrogen atoms in **1**−**3** and **6** were positioned geometrically and constrained to ride on their parent atoms, with O−

dx.doi.org/10.1021/ic302105a | Inorg. Chem. 2013, 52, 3663−3673

H = 0.84 Å, C−H = 0.95−1.00 Å, and U_{iso} = 1.2−1.5U_{eq} (parent atom). In **4** the idealized positions of the OH hydrogens for oxygen atoms O1−O6 were estimated with *HYDROGEN*[17] program and constrained to ride on their parent atom with U_{iso} = 1.5 (parent atom). The H_2O hydrogen atoms were positioned manually and were constrained to ride on their parent atom O11, with U_{iso} = 1.5U_{eq} (parent atom). All other hydrogen atoms were positioned geometrically as in **1**−**3**, **6**. The crystallographic details are summarized in Tables 1 and S1 (Supporting Information).

Photophysical Measurements. All photophysical measurements were carried out in acetonitrile, which was distilled prior to use. All solutions were carefully degassed before lifetime and quantum yield measurements. The light-emitting diode (LED; maximum emission at 385 nm) was used to pump luminescence. The LED was used in continuous and pulse mode (pulse width, 1−20 μs; duty of edge, ∼90 ns; repetition rate, 100 Hz to 10 kHz). A digital oscilloscope Tektronix TDS3014B (Tektronix, bandwidth 100 MHz), monochromator MUM (LOMO, interval of wavelengths 10 nm), and photomultiplier tube Hamamatsu were used for lifetime measurements. Emission and excitation spectra were measured on a Varian Cary Eclipse spectrofluorimeter. The absolute emission quantum yield was determined by the comparative method using LED pumping and rhodamine 6G in ethanol (Φ_{em} = 0.95 ± 0.03) as standard with the refraction coefficients of acetonitrile and ethanol equal to 1.34 and 1.36, respectively.[18]

Computational Details. The Au^I−Ag^I clusters **1**−**6** were studied using the hybrid PBE0 density functional.[19] The gold and silver atoms were described by a triple-ζ-valence quality basis set with polarization functions (def2-TZVP).[20] Scalar relativistic effects were taken into account by applying 28-electron and 60-electron relativistic effective core potentials for Ag and Au, respectively.[21] A split-valence basis set with polarization functions on non-hydrogen atoms was used for all the other atoms.[22] To facilitate comparisons with the experiments, point group symmetry was applied as follows: **1**−**3**, C_i; **4**−**6**, D_3. The geometries of the complexes **4**−**6** were fully optimized, while for the complexes **1**−**3** with very flexible frameworks the phosphorus atoms were fixed at the experimentally determined positions and the other atoms were allowed to relax. The excited states were investigated with the time-dependent DFT approach.[23] The singlet excitations were determined at the optimized ground state S_0 geometries, while the lowest energy triplet emissions were determined at the optimized T_1 geometry. All electronic structure calculations were carried out with the TURBOMOLE program package (version 6.3).[24]

RESULTS AND DISCUSSION

Synthesis and Characterization. The preparative methodology employed is closely analogous to a well established method leading to the families of octanuclear Au^I−M^I (M = Cu^I, Ag^I) clusters $[Au_6M_2(C_2Ar)_6(PP)_3]^{2+}$ (PP = diphosphine) and involves treatment of the $(AuC_2Ar)_n$ polymeric acetylides with a phosphine ligand and corresponding M^+ ions.[5b,7c] Depolymerization of $(AuC_2Ph)_n$ with 1,4-bis-(diphenylphosphino)butane (PbuP) and addition of stoichiometric amount of $AgPF_6$ gives yellow-greenish solution, which contains several compounds according to ^{31}P NMR spectroscopic data. However, upon standing for 24 h some color fading was observed, and after a brief work up and consequent recrystallization the novel $[Au_{12}Ag_4(C_2Ph)_{12}(PbuP)_6]^{4+}$ cluster (**1**) was isolated in good yields as a yellow crystalline material (Scheme 2).

Its structure in the solid state was determined by an X-ray diffraction study (Figure 1, an ORTEP view is shown in Figure S1 in the Supporting Information). The ESI mass spectrum of **1** (Figure S2) displays the main signal of the quadruply charged cation at m/z 1640.1, the isotopic pattern of which completely fits the stoichiometry of the $[Au_{12}Ag_4(C_2Ph)_{12}(PbuP)_6]^{4+}$ molecular ion.

Scheme 2. Assembly of the Clusters 1−6[a]

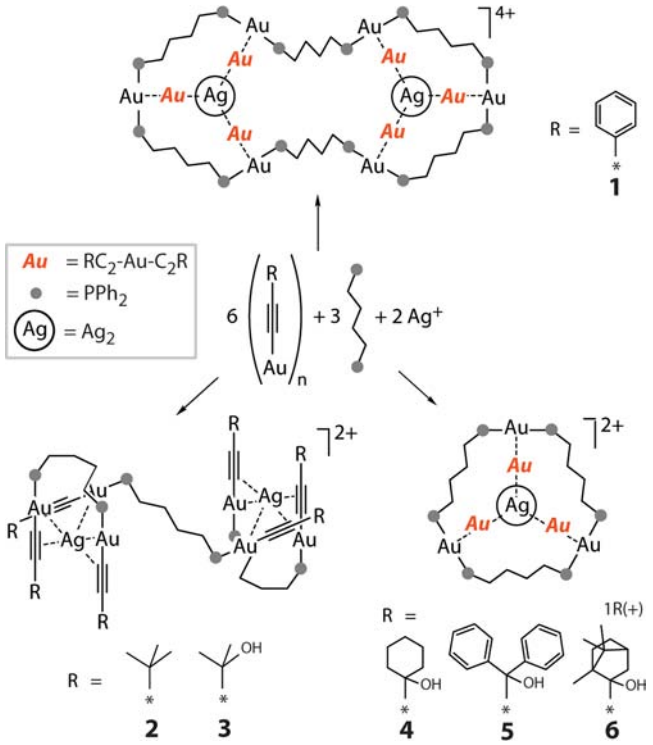

[a] CH_2Cl_2/acetone, 298 K, 4-24 h, yields 74-93%.

The molecule consists of two heterometallic alkynyl clusters $[Au_3Ag_2(C_2Ph)_6]^-$ embedded into the $[Au_6(PbuP)_6]^{6+}$ gold-diphosphine "belt" and held together by the Au−Au interactions enhanced by the electrostatic attraction between the central anionic clusters and the cationic metallacycle. The $[Au_6(PbuP)_6]^{6+}$ fragment adopts a "chair"-like conformation (Figure 1) and provides considerable spatial separation of two entrapped cluster cores. The general structural motif, $\{Au_3Ag_2\}$ framework inside a $\{Au(PP)\}_n$ "belt", was described earlier.[7c,9] However, this double cluster arrangement and the nuclearity are unprecedented. The Au−Au distances fall in the range typical for the related compounds and for the aurophilic interactions in general.[2b] The Au−Ag contacts within the identical $\{Au_3Ag_2\}$ cores (2.8734(6)−3.0503(7) Å) are significantly shorter than the sum of the corresponding van der Waals radii (3.38 Å) and are similar to the intermetallic separations determined for other Au−Ag compounds.[7c,8a,9]

When the synthetic protocol used to obtain **1** was applied to the $(AuC_2R)_n$ (R = Bu^t, C_3H_7O) acetylides, the $[Au_6Ag_2(C_2R)_6(PbuP)_3]^{2+}$ complexes (**2**, **3**) were isolated as colorless crystalline solids (Scheme 2). The XRD analysis revealed their solid state structures, shown in Figure 2 (see Figure S3 for the corresponding ORTEP views). The ESI-MS of **2** and **3** display the signals, corresponding to the doubly charged molecular cations (at 1580.25 and 1586.17, respectively, Figure S2). However, the intensity of these signals were rather low in comparison to those of the fragmented species.

Molecular ions of **2** and **3** adopt an unprecedented structural motif, which involves three neutral $(RC_2Au)PbuP(AuC_2R)$ molecules assembled together *via* coordination of the —C≡CR units to Ag^I ions in π-bridging mode and Au−Ag metallophilic interactions. Each silver ion is connected to three gold(I)-alkynyl fragments, which in turn are "capped" by three

dx.doi.org/10.1021/ic302105a | Inorg. Chem. 2013, 52, 3663−3673

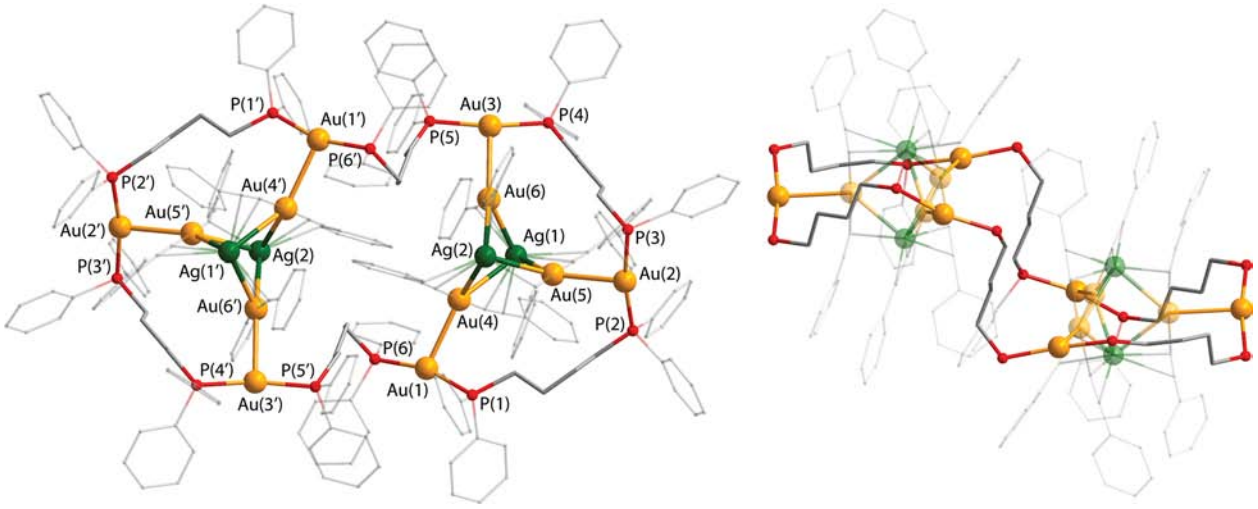

Figure 1. Molecular view of the tetracation **1**. Right shows side view (phenyl rings of the diphosphines omitted). Selected interatomic distances (Å): Au(1)−Au(4) 2.9244(4), Au(2)−Au(5) 2.9360(4), Au(3)−Au(6) 2.9409(4), Ag(1)−Au(4) 2.9935(6), Ag(1)−Au(5) 2.9787(6), Ag(1)−Au(6) 2.9031(6), Ag(2)−Au(4) 3.0503(7), Ag(2)−Au(5) 2.8734(6), Ag(2)−Au(6) 2.9459(6). Symmetry transformations used to generate equivalent atoms: 1.5 − *x*, 0.5 − *y*, 2 − *z*.

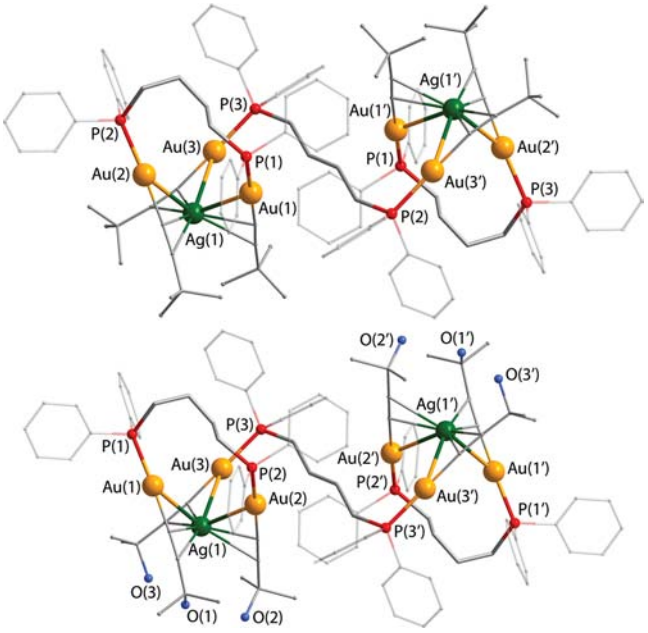

Figure 2. Molecular views of the dications **2** (top) and **3** (bottom). Selected interatomic distances (Å) in **2**: Au(1)−Ag(1) 3.0342(4), Au(2)−Ag(1) 3.0272(4), Au(3)−Ag(1) 3.1268(4), P(1)−Au(1) 2.2740(11), P(2)−Au(2) 2.2805(11), P(3)−Au(3) 2.2738(11). Symmetry transformations used to generate equivalent atoms: 1 − *x*, 1 − *y*, 1 − *z*. In **3**: Au(1)−Ag(1) 3.1191(9), Au(2)−Ag(1) 2.9605(9), Au(3)−Ag(1) 3.1918(10), P(1)−Au(1) 2.278(3), P(2)−Au(2) 2.262(3), P(3)−Au(3) 2.271(3). Symmetry transformations used to generate equivalent atoms: 1 − *x*, 1 − *y*, 1 − *z*.

phosphorus atoms of the phosphines, to give structural motif similar to that found earlier for the heterometallic complexes based on a rigid triphosphine ligand.[25] Indeed, in the compounds under study the "$(AuC_2R)_3Ag$" fragments are stabilized by the interaction with two phosphorus atoms of the bridging diphosphine and with the third phosphorus atom from the ligand linking two tetranuclear clusters $\{Au_3Ag\}$. The Au−Ag distances in both **2** and **3** (3.0272(4)−3.1268(4) Å and 2.9605(9)−3.1918(10) Å, respectively) are within the range typical for the Au−Ag compounds[7c,8a,9] and on average are slightly longer than those in **1**. Coordination of silver ions in **3** is less symmetrical than in **2** that is indicated by the larger dispersion of the intermetallic contacts. The shortest Au−Au separation in these clusters exceeds 4.1 Å that is considerably longer than the sum of Au van der Waals radii (3.32 Å) that points at the absence of gold−gold interactions. It is worth noting that in **3** the distance between O(1) and O(2) atoms of the hydroxyl groups is 2.911 Å that suggests the presence of effective O···H−O hydrogen bonding within the central tri(gold-alkynyl) unit. This local intramolecular interaction additionally distorts the symmetry of the "$(AuC_2R)_3Ag$" cluster unit.

The structural difference between **1** and **2**, **3** prompted us to further investigate of the alkynyl group effect on the self-assembly processes in these systems. Thus, the use of hydroxyaliphatic acetylides $(AuC_2R)_n$ (R = $C_6H_{11}O$, $C_{13}H_{11}O$, 1*R*(+)-$C_{10}H_{17}O$) in the reactions under study (Scheme 2) leads to the complexes of the same composition as that found for **2** and **3**: $[Au_6Ag_2(C_2R)_6(PbuP)_3]^{2+}$, which were isolated as yellow crystalline solids (**4**, **5**, and **6**). The XRD study of **4** and **6** showed that these clusters belong to a different structural type (Figure 3), similar to that reported for the Au^I−Ag^I complex based on PPh_2−C_2−C_2−PPh_2 ligand.[7c] Complex **5** did not give crystals of suitable quality, and its structure was estimated on the basis of NMR spectroscopic studies (see below). The mass spectra of **4**−**6** exhibit dominating signals at 1706.27, 1958.25, and 1868.40, respectively, which fit the proposed composition of doubly charged molecular cations (Figure S2).

The complexes **4** and **6** consist of the bimetallic alkynyl clusters $\{Au_3Ag_2\}$ wrapped about by the triangular gold-diphosphine "belt" $[Au_3(PbuP)_3]^{3+}$. The Au−Au contacts between the central and external fragments lie in the range 2.7936(4)−2.8771(6) Å and therefore are very close to the values found in **1** and the related complexes.[9] The heterometallic contacts are also similar to those determined in other Au−Ag alkynyl clusters including **1** and are slightly shorter than the metal−metal distances found in **2** and **3**, which have less stereochemically strained structure. The O−O

dx.doi.org/10.1021/ic302105a | *Inorg. Chem.* 2013, 52, 3663−3673

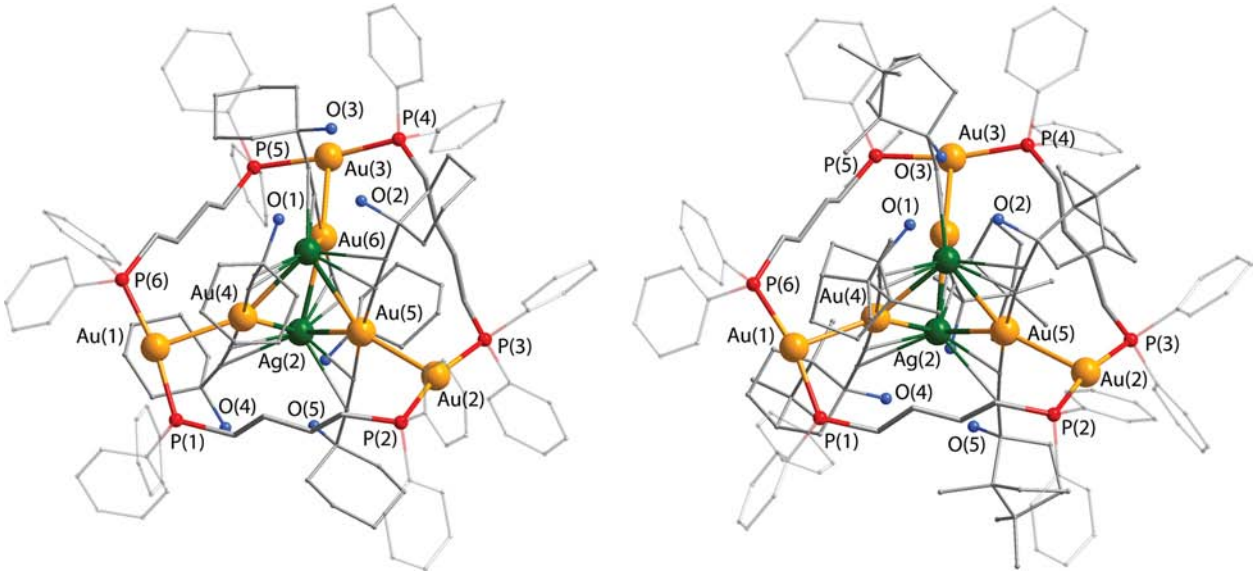

Figure 3. Molecular view of the dications **4** (left) and **6** (right, one of two independent molecules is shown). Selected interatomic distances (Å) in **4**: Au(1)−Au(4) 2.8363(4), Au(2)−Au(5) 2.7936(4), Au(3)−Au(6) 2.8539(4), Ag(1)−Au(4) 2.9405(5), Ag(1)−Au(6) 3.0362(5), Ag(1)−Au(5) 3.0820(6), Ag(2)−Au(6) 2.9665(5), Ag(2)−Au(5) 3.0318(6), Ag(2)−Au(4) 3.0413(5). In **6**: Au(1)−Au(4) 2.8344(6), Au(2)−Au(5) 2.8771(6), Au(3)−Au(6) 2.8208(5), Ag(1)−Au(4) 2.9132(8), Ag(1)−Au(6) 2.9678(7), Ag(1)−Au(5) 2.9990(8), Ag(2)−Au(5) 2.9281(8), Ag(2)−Au(6) 2.9463(8), Ag(2)−Au(4) 3.0181(7).

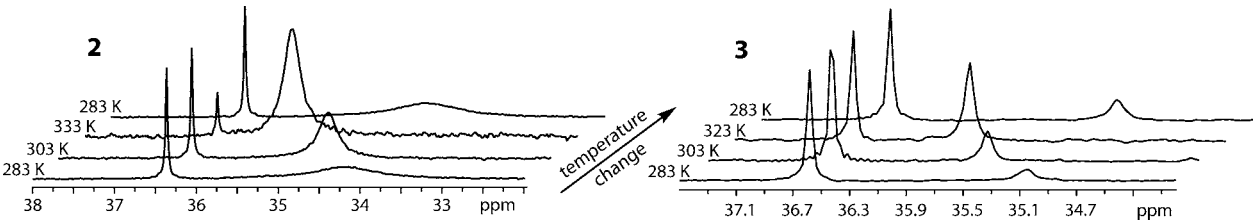

Figure 4. Variable temperature ^{31}P NMR spectra of **2** (left) and **3** (right) in acetonitrile-d_3.

separations in **4** and **6** range from 2.688 to 2.793 Å (except two elongated distances O(1)−O(3) and O(4)−O(6) exceeding 3.85 Å) that indicates the presence of O···H−O hydrogen bonding stabilizing the "Au_3Ag_2" central framework.

NMR Spectroscopic Study. The NMR investigation of the complexes under study showed that "loosely packed" clusters **1**−**3** demonstrate complicated dynamic behavior related to interconversion of different isomeric forms shown in Scheme 2. The spectroscopic data obtained for complexes **4**−**6** indicate that the "rods-in-belt" motif is the most probable structural pattern these compounds adopt in solution. Solid state structure of this type has been revealed for **4**, and its ^{31}P and ^{1}H NMR data are completely compatible with this structural hypothesis. The ^{31}P NMR spectrum of **4** at 283 K displays a singlet resonance of all-equivalent phosphorus atoms of the diphosphine ligands at 35.4 ppm together with the PF_6^- septuplet at −144.6 ppm that fits the D_3 symmetry group the "rods-in-belt" molecule belongs to. It is worth noting that this complex is thermally stable and warming of its acetonitrile solution up to 323 K gave only trace amount of another isomeric form, see Experimental Section. The low temperature ^{1}H NMR data are also compatible with this structural pattern. For example, the proton spectrum of **4** in the low field area contains a set of signals corresponding to the ortho−meta−para protons (7.8−7.4 ppm) of the diphosphine phenyl rings. The position and structure of the corresponding multiplets are typical for the complexes of this family.[4d,5b] The signals of the alkynyl ligand hydroxyl protons appear at 4.79 ppm, whereas the high field part displays the signals of the diphosphine methylene spacers together with a set of resonances assigned to the cyclohexyl moiety. The ^{31}P NMR spectra of **5** and **6** in CD_3CN at 303 and 283 K, respectively, also display a major singlet resonance of the coordinated phosphorus atoms (36.0 and 35.8 ppm) accompanied by the minor signals at 34.7 and 36.6 ppm. The major signals, which remain narrow in the temperature range 283−323 K, may be assigned to the rigid "rods-in-belt" structural motif. In fact, the ^{1}H spectra (major components) of **5** and **6** also fit well this type of molecular symmetry to give standard sets of signals corresponding to all-equivalent alkynyl ligands including singlets of hydroxyl protons, two signals of methylene spacers, and ortho−meta−para resonances of the phosphine phenyl protons (see Experimental Section and Figure S5). The duplication of the proton signals of **6** in the aromatic area of the proton spectrum is evidently due to diastereotopic position of the phenyl rings in this molecule. Along with these groups of signals the broadened resonances of the minor structural forms are also observed, which however do not prevent interpretation of the major spectroscopic pattern. It has to be noted that warming of the solution of **5** results in irreversible degradation of the major isomeric form; this process also effects the photophysics of this system, *vide infra*.

Another group of compounds, complexes **2** and **3**, which in the solid state form the structural patterns shown in Scheme 2

dx.doi.org/10.1021/ic302105a | *Inorg. Chem.* 2013, 52, 3663−3673

and Figure 2 with two loosely packed "$(AuC_2R)_3Ag$" fragments, display dynamic equilibrium in solution between two isomers. Reversible transformation of these isomeric forms is clearly illustrated by the VT ^{31}P spectra of **2** and **3** (Figure 4).

For example, the spectra of these complexes in CD_3CN at 283 K display narrow low field signals and broadened high field resonance of another isomer. Heating of these solutions results in narrowing of the high field signals and growth of their relative intensities, cooling down the mixture returns the system to the initial state. These spectroscopic variations correspond to a relatively slow (in the NMR time scale) dynamics, which can be ascribed to the equilibrium between the "rods-in-belt" form of these complexes (type I, analogues of **4**–**6**, the narrow low-field signals) and the one found in the solid state (type II, broaden high-field signals), Scheme 3.

Scheme 3. Proposed Temperature Dependent Interconversion of the Isomeric Forms of 2 and 3

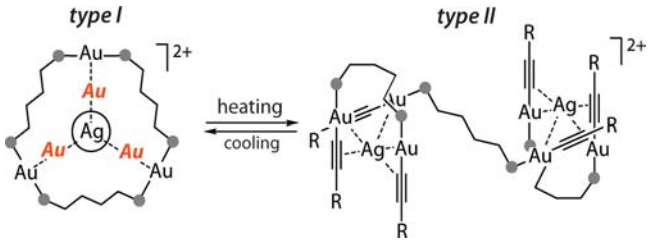

This hypothesis is also confirmed by the previously reported data, showing that the signals of the "P–Au–P" fragments (i.e., those found in **4**–**6** clusters of type I) appear in a lower field region of the spectrum in comparison to the resonances corresponding to "P–Au–C_2R" units (i.e., found in **2**, **3**, type II) for the same phosphine ligand.[4d,7b,26] The narrow resonances, which dominate in the low temperature spectra, can be tentatively assigned to the type I structures, whereas the other broadened signals may be assigned to the stereochemically nonrigid structural pattern revealed in the solid state (type II). The intramolecular scrambling in the latter isomeric form is clearly visible in the set of VT ^{31}P spectra of **2** (Figure 4). The high temperature (333 K) spectrum shows major (10/1) broadened signal corresponding to the dominant type II stereochemically nonrigid species. Though it approaches the high temperature limit, it still displays some broadening of the ^{31}P signal. This type of variable temperature behavior is indicative of a scrambling process, which makes equivalent the phosphorus atoms of inherently asymmetric structures shown in Figure 2. A feasible mechanism of the relevant dynamics may consist of reversible coordination–dissociation of the –Au–C_2R fragments to/from Ag^I ions and related movement of the $(R_2CAu)_2(PbuP)$ fragments from the intracluster bridging mode to the linking intercluster position (Scheme 4).

The effect of this dynamics is particularly visible in the ^1H spectrum of **2** at 333 K (Figure S6) where two multiplets of the phosphine phenyl rings (7.63 *ortho* protons and AB system of *meta*–*para* protons at ca. 7.5 ppm), two signals of methylene spacers at 2.5 and 1.7 ppm, and the signal of the alkynyl methyl groups at 1.35 ppm testify in favor of the scrambling process, which makes equivalent all alkynyl and phosphine ligands in the asymmetric structural pattern revealed in the solid state structure. The variable temperature behavior of the ^{31}P spectra of **3** is analogous to that observed for **2**, and it is sensible to assign the narrow low field signal dominating at low

Scheme 4. Proposed Mechanism of the Solution Dynamics of Compounds 2 and 3

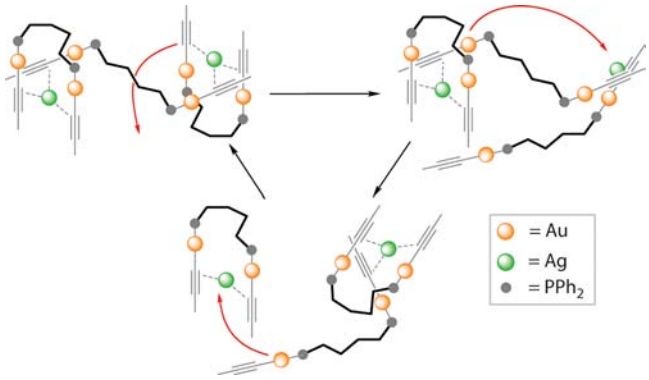

temperature to the "rods-in-belt" structure (analogue of **4**–**6**, type I), whereas the broadened high field resonance can be similarly ascribed to the type II structure found in the solid state. Analysis of the proton spectrum of **3** at 283 K showed that the major set of signals fits well the "rods-in-belt" structural hypothesis to give the usual set of resonances corresponding to D_3 symmetry group of this species, see Experimental Section.

Complex **1** displays the most complicated behavior in solution. The VT ^{31}P spectra of this complex (Figure S7) show the presence of several isomeric forms, and the tentative structural assignment of which might include the isomer revealed in the solid state as well as its possible conformations (as indicated by the dominating signal in the ESI-MS), the "rods-in-belt" molecules, and other intermediate species of unknown structure. Their interconversion upon temperature variations results in related changes of emission characteristics of the solution under study, which will be discussed below.

Photophysical Properties. Spectroscopic and photophysical data for **1**–**6** are given in Table 2. The solution and the solid state emission spectra are shown in Figures 5 and S8 (Supporting Information), respectively. The excitation spectra are shown in Figure S9. It has to be noted that solution data for **1**–**3** should be analyzed taking into account dynamic equlibria between various structural isomers of these complexes presented in acetonitrile solution, see above. On the contrary, the room and low temperature data for **4**–**6** according to the NMR measurements are related to the only isomeric form ("rods-in-belt" structural pattern), which dominates in solution in this temperature range.

Complexes 4–6. Absorption spectra of this group of complexes display two equally strong bands at about 275 and 370 nm. The high energy bands are evidently generated by metal-perturbed IL (both alkynyl and phosphine ligands) transitions, whereas the long wavelength absorption is related to electron transfer between orbitals localized mainly inside the "$Ag_2Au_3(C_2R)_6$" cluster core, see also Computational Details section. All three complexes are bright blue emitters with emission band maxima at 490, 472, and 471 nm, respectively. As expected the luminescence wavelengths for **4**–**6** are considerably blue-shifted compared to those of the Au–Cu congeners; for example, the copper analogue of **4** displays orange emission with the maximum at 590 nm.[10] The high energy shift of the silver complexes emission is due to lower energy of the highest occupied molecular orbitals in silver containing complexes compared to those of the copper relatives. All complexes display single exponential emission

dx.doi.org/10.1021/ic302105a | Inorg. Chem. 2013, 52, 3663–3673

Table 2. Photophysical Properties of 1−6 in Solution (298 K, λ_{ex} = 386 nm) and in the Solid State

	solution (acetonitrile)						solid state			
	λ_{ab}/nm (10^{-3} ε/M^{-1} cm^{-1})[a]	λ_{ex} /nm[b]	λ_{em}/nm[b]	Φ[c] (aerated/degassed)	τ_{obs}/μs[b] (aerated/degassed)	Stokes shift/nm	λ_{em}/nm	τ_{obs}/μs	λ_{ex}/nm[b]	Stokes shift/nm
1	267 (159.2); 280 (159.2); 347 (56.4)	322; 379	491	0.04/0.05	0.22/0.21	112	494	0.66	339; 419	74
2	272 (15.3); 369 (4.61)	284; 369	472	0.10/0.57	0.43/0.28	103	490	0.67	<270; 379	97
3	273 (4.99); 370 (2.90)	<270; 374	502	0.10/0.45	0.71/0.39	128	509	0.94	<270; 369	125
4	275 (4.08); 372 (2.72)	298; 333; 399	490	0.21/0.65	0.92/0.54	91	500	0.97	339; 366; 414	78
5	275 (30.3); 378 (43.8)	276; 377	472	0.63/0.73	1.51/1.39	95	496	0.99	340; 365; 414	66
6	274 (31.4); 369 (42.4)	284; 369	471	0.55/0.76	1.28/0.78	102	489	0.50	339; 366; 408	61

[a]Measured at 283 K. [b]λ_{ex}, $\lambda_{em.}$, τ_{obs} are not temperature dependent and were measured at 298 K. [c]Quantum yields measured at 298 K.

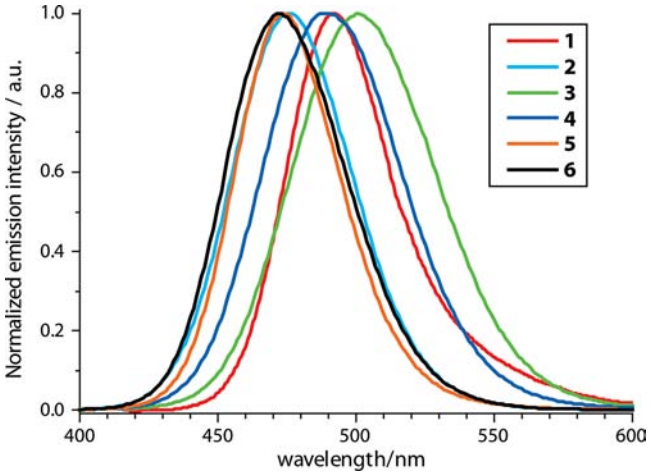

Figure 5. Normalized emission spectra of **1−6** in acetonitrile (298 K, λ_{ex} = 386 nm).

decay with the excited state lifetime in microsecond domain. This observation together with substantial Stokes shift is indicative of luminescence from the triplet excited state localized in the cluster core that is typical for the well characterized "rods-in-belt" supramolecular aggregates.[4d,5b] On warming the complexes **4−6** show behavior which is compatible with the data obtained using ^{31}P NMR spectroscopy, see NMR Spectroscopic Study section. Thermally stable complexes **4** and **6** showed slight and reversible changes in emission intensity, whereas **5** irreversibly yields a product which does not display appreciable emission.

Complexes 2 and 3. The VT ^{31}P study for the complexes **2** and **3** also indicated reversible dynamic equilibria between "rods-in-belt" aggregates (type I) stable at low temperature and "loosely packed" type II structures (see Scheme 3), which dominate in solution at higher temperature. According to the data obtained previously, the type I compounds are extremely effective triplet luminophors with the phosphorescence quantum yield (QY) in many cases exceeding 80%. As discussed above, the structure of the $\{Au_3Ag\}$ cluster frameworks in type II species is essentially similar to that found in Au−Cu complexes based on the tridentate phosphine, $[tppm(AuC_2R)_3Cu]^+$ (tppm = tris(diphenylphosphino)-methane),[25] which exhibit luminescence at least an order of magnitude weaker compared to the "rods-in-belt" complexes of type I. Provided that emission efficiency of the type II isomeric forms of **2** and **3** (Scheme 3) is essentially similar to that found for the compounds based on the tridentate phosphine $[tppm(AuC_2R)_3Cu]^+$, the temperature growth should lead to a significant decrease of intensity of the main luminescence band and probably some shift of the maximum position. The results obtained are completely compatible with this hypothesis to give a reversible decrease in emission intensity (see Figure 6C) for approximately an order of magnitude while warming solution from 283 up to 323 K, which is accompanied by the equilibrium shift to the weakly emissive isomers. Cooling the solution back to 283 K results in successful return of luminescence intensity, Figure 6.

Under the framework of this model, the emission parameters given in Table 2 (298 K) for **2** and **3** can be considered as characteristics corresponding to type I complexes, except for the QY, which in fact is related to a part of the molecules converted into this emissive isomer. Thus, the "rods-in-belt" type I isomers of **2** and **3** are effective triplet emitters, which also display only weak luminescence quenching with molecular

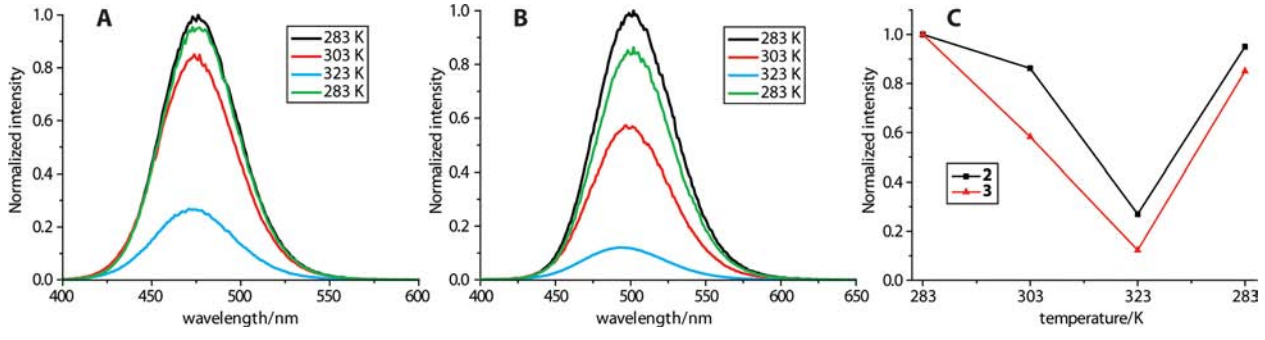

Figure 6. VT luminescence spectra of **2** (A) and **3** (B); temperature dependence of emission intensity (C) (acetonitrile, λ_{ex} = 386 nm).

dx.doi.org/10.1021/ic302105a | Inorg. Chem. 2013, 52, 3663−3673

oxygen (see Table 2) similar to the other compounds of this class. Unfortunately, due to weak emission of the type II isomer (below the noise level) we are unable to separate and calculate its photophysical characteristics.

The solid-state emission maxima for both type I and type II clusters are essentially similar despite different structural arrangements found for the corresponding complexes in crystals. This observation is in line with the photophysical data reported for the "rods-in-belt" Au–Cu clusters bearing PbuP ligand (analogues of type I compounds)[10] and [tppm-$(AuC_2R)_3Cu]^+$ complexes (congeners of type II compounds)[25] having the same alkynyl groups. These species exhibit nearly identical emission wavelengths (alkyne = $-C_2Ph$, 565 and 560 nm, respectively), but the latter tetranuclear clusters show dramatically lower QY (66% vs 1.7%).

According to the ^{31}P NMR measurements, complex **1** showed extremely complicated dynamic behavior in solution, with more than three species of different nature being involved in this process (Figure S7). Taking into account mass-spectroscopic data that show the dominating signal of the molecular ion matching the composition of **1** found in the solid state, it seems probable that one of the major species existing in solution is the crystallographically characterized aggregate and its possible conformations, which give the principal contribution into the emission observed. Because the emission band is symmetrical and displays monoexponential decay we can tentatively ascribe the emission parameters observed (Table 2) to this form of compound **1**. A lower quantum yield of **1** in comparison to the other clusters of this family can be rationalized using quantum chemical calculation (vide infra), which points to a smaller contribution of the Au and Ag ions to the lowest excited states. That in turn decreases spin–orbital coupling and consequently the rate of the radiative triplet–singlet transition. Additionally, in solution there are a few forms of the complexes, not all of which are bright luminophors that also cause a drop in the emission intensity.

Computational Studies. We also investigated the structural and photophysical characteristics of the supramolecular Au^I–Ag^I complexes **1**–**6** with quantum chemical methods. The geometries of the studied complexes were first optimized at the PBE0-DFT level of theory, enabling comparisons to the experimental X-ray structures for complexes **1**–**4** and **6**. In the case of complexes **1**–**3** with rather flexible frameworks, we could only investigate the structures determined in the solid state by fixing the phosphorus atoms at the experimentally determined positions and optimizing the positions of the other atoms. The important metal–metal distances in the resulting optimized structures correlate reasonably well with the experimental parameters. For example, the Au–Au and Au–Ag bond lengths in **1** are in the ranges 2.97–3.02 Å (exp 2.92–2.94 Å) and 2.93–3.11 Å (exp 2.87–3.05 Å), respectively (see Table S2 in the Supporting Information for a full listing of the intermetallic distances). In the case of the "rods-in-belt" complexes **4**–**6**, it was not necessary to fix any atom positions during the structural optimization. The metal–metal distances in the resulting structures are in good agreement with the X-ray structures (for instance, Au–Au distances in **6**: 2.88 Å vs 2.82–2.87 Å, see Table S2 for full details).

The photophysical results obtained for complexes **1**–**6** at the PBE0-TDDFT level of theory are listed in Table 3. For complexes **2** and **3**, the photophysical data listed in Table 3 refers to the "rods-in-belt" (type I) structures. For all

Table 3. Computational Photophysical Results for the Au^I–Ag^I Clusters 1–6 (PBE0 TD-DFT)

	λ_{ab} $S_0 \rightarrow S_1$ (nm)		λ_{ab} $S_0 \rightarrow S_2$ (nm)		λ_{em} $T_1 \rightarrow S_0$ (nm)	
complex	theor[a]	exp	theor	exp	theor	exp
1[b]	357 (0.19)	347		267	477	491
2[c]	362 (0.64)	369	287 (0.15)	272	437	472
3[c]	375 (0.73)	370	286 (0.26)	273	462	502
4	376 (0.57)	372	287 (0.24)	275	461	490
5	374 (0.84)	378	279 (0.20)	275	467	472
6	371 (0.28)	369	276 (0.10)	274	448	471

[a]Wavelenghts in nm, oscillator strengths given in parentheses. [b]Investigation of the $S_0 \rightarrow S_2$ excitation not feasible due to the large size of the structure; $T_1 \rightarrow S_0$ emission wavelength calculated at the S_0 geometry. [c]Computational photophysical data for the "rods-in-belt" (type I) structure.

complexes, the predicted $S_0 \rightarrow S_1$ and $S_0 \rightarrow S_2$ singlet excitation energies are in accordance with the experimental absorption maxima. The corresponding excited state transition densities are plotted for complex **6** in Figure 7 (for the transition densities of the other complexes, see the Supporting Information, Figures S10 and S11). For the "rods-in-belt" structures, the lowest energy singlet excitation arises from the central metal core, while the higher energy singlet excitation is a metal-perturbed intraligand excitation involving both the alkynyl and phosphine ligands. In the case of complex **1**, the lowest energy singlet excitation involves contributions from both the alkynyl ligands and the metal atoms.

The predicted $T_1 \rightarrow S_0$ emission energies are also in line with the experimental values, although the differences from the experiment are larger than those for the excitation energies. For the "rods-in-belt" structures, the triplet emission is clearly metal-centered. The strong involvement of the Au atoms in the lowest energy excited states facilitates the spin-forbidden singlet–triplet intersystem crossing,[27] leading to the observed efficient phosphorescence. In the case of complex **1** showing clearly lower quantum yields for degassed samples, the contribution from the metal atoms is smaller and the alkynyl ligands play a much larger role in comparison to the "rods-in-belt" structures. The decreased importance of the heavy gold atoms is likely to result in less efficient intramolecular energy transfer between the emissive singlet and triplet excited states.

We also investigated the photophysical characteristics of the type II structures of the complexes **2** and **3**, which were found to be weak emitters. In this case, the gold atoms play only a very minor role in the lowest energy excitation and the triplet emission is actually centered on the phosphine ligand (Figure S10). The intraligand nature of the lowest energy triplet emission is very probably the reason for poor luminescence of type II clusters **2** and **3** in solution.

CONCLUSION

In summary, a family of novel intensely luminescent Au^I–Ag^I alkynyl-diphosphine clusters was obtained according to a self-assembly protocol that involves treatment of the homoleptic $(AuC_2R)_n$ precursors with stoichiometric amounts of bis-(diphenylphosphino)butane (PbuP) ligand and Ag^+ ion (R = Ph (**1**), Bu^t (**2**), 2-propanolyl (**3**), 1-cyclohexanolyl (**4**), diphenylmethanolyl (**5**), 2-borneolyl (**6**)). The complexes adopt three different structural arrangements depending on the nature of the alkynyl ligand. The unprecedented

dx.doi.org/10.1021/ic302105a | Inorg. Chem. 2013, 52, 3663–3673

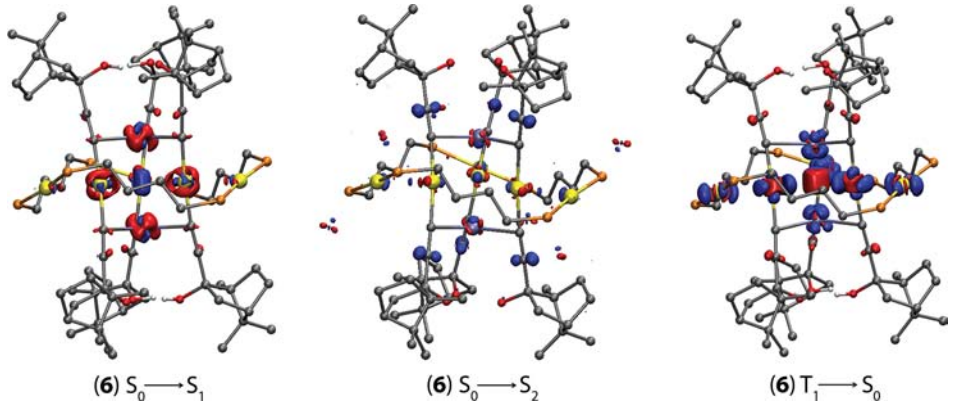

Figure 7. Transition densities for the two lowest energy singlet excitations ($S_0 \rightarrow S_1$ and $S_0 \rightarrow S_2$) and the lowest energy triplet emission ($T_1 \rightarrow S_0$) of the complex **6** (isovalue 0.002 au). Hydrogen atoms and phenyl rings omitted for clarity. During the transition, the electron density increases in the blue areas and decreases in the red areas. For the $S_0 \rightarrow S_2$ transition, the electron density clouds close to the phosphorus atoms arise from the diphosphine-based phenyl rings (not drawn here).

hexadecanuclear cluster **1** (R = Ph) contains two heterometallic units $[Au_3Ag_2(C_2Ph)_6]^-$ embedded into the gold-diphosphine cycle $[Au_6(PbuP)_6]^{6+}$, while the complexes with aliphatic alkynes have a general composition of $[Au_6Ag_2(C_2R)_6(PbuP)_3]^{2+}$ and give two isomeric forms in the solid state (type I (**4**–**6**); type II (**2**, **3**)) as found by an X-ray crystalographic study.

Complexes **1**–**6** were characterized in detail by NMR spectroscopy to reveal complicated behavior of **1**–**3** in solution related to interconversion of possible conformations (**1**) of different isomeric forms (**2**, **3**: type I and type II). The spectroscopic data obtained for the complexes **4**–**6** indicate that the motif found in the solid state (type I) is the most probably retained in solution.

All the titled compounds exhibit sky-blue room temperature phosphorescence in solution and in the solid state in the spectral range 471–509 nm with maximum quantum yield of 76% (**6**, in solution). The structural type has small effect on the emission maximum, but dramatically influences the intensity of luminescence, which is most effective for the type I clusters **4**–**6**. Phosphorescence of these complexes displays low sensitivity to O_2 quenching due to the efficient shielding of the chromophoric polymetallic centers by the organic ligand environment.

The DFT computational studies revealed the difference in photophysical behavior of the structural types described. Thus, for type I complexes the triplet emission is metal-centered with strong involvement of the Au atoms. In the case of the tetracationic complex **1**, the contribution from the metal atoms is smaller leading to lower quantum yield. In the type II clusters **2** and **3**, which were found to be weak emitters, the gold atoms play only a very minor role in the lowest energy excitation and the triplet emission is actually centered on the phosphine ligand that is very probably the reason of poor luminescence.

■ ASSOCIATED CONTENT

Supporting Information

X-ray crystallographic data in CIF format for **1**–**4**, **6**; ESI mass spectra of **1**–**6**, additional NMR spectroscopic data; additional computational results; optimized Cartesian coordinates of the studied systems in atomic units. This material is available free of charge via the Internet at http://pubs.acs.org.

■ AUTHOR INFORMATION

Corresponding Author

*E-mail: igor.koshevoy@uef.fi (I.O.K.), stunik@inbox.ru (S.P.T.).

Notes

The authors declare no competing financial interest.

■ ACKNOWLEDGMENTS

This research has been supported by the strategic funding of the University of Eastern Finland (Russian-Finnish collaborative project and Spearhead project), Saint-Petersburg State University research grant 12.37.132.2011, the Academy of Finland (grant 138560/2010, A.J.K.), and Russian Foundation for Basic Research (grants 11-03-00541-a, 11-03-00974-a, 11-03-92010-HHC_a). The work was performed using the unique installation "Laser tweezers" with financial support of the Ministry of Education and Science of the Russian Federation (State Agreement No. 14.518.11.7034).

■ REFERENCES

(1) (a) Schmidbaur, H.; Schier, A. *Chem. Soc. Rev.* **2012**, *41*, 370–412. (b) Silvestru, C., Gold–Heterometal Interactions and Bonds. In *Modern Supramolecular Gold Chemistry*; Laguna, A., Ed.; Wiley-VCH: Weinheim, 2008; pp 181–295.

(2) (a) Pyykko, P. *Chem. Rev.* **1997**, *97*, 597–636. (b) Pyykkö, P. *Chem. Soc. Rev.* **2008**, *37*, 1967–1997.

(3) (a) Gimeno, M. C.; Laguna, A. *Chem. Soc. Rev.* **2008**, *37*, 1952–1966. (b) Jia, J.-H.; Wang, Q.-M. *J. Am. Chem. Soc.* **2009**, *131*, 16634–16635. (c) Che, C.-M.; Lai, S.-W., Luminescence and Photophysics of Gold Complexes. In *Gold Chemistry*; Mohr, F., Ed.; Wiley-VCH: Weinheim, 2009; pp 249–282. (d) Strasser, C. E.; Catalano, V. J. *J. Am. Chem. Soc.* **2010**, *132*, 10009–10011. (e) Lasanta, T.; Olmos, M. E.; Laguna, A.; Lopez-de-Luzuriaga, J. M.; Naumov, P. *J. Am. Chem. Soc.* **2011**, *133*, 16358–16361. (f) He, X.; Yam, V. W.-W. *Coord. Chem. Rev.* **2011**, *255*, 2111–2123. (g) Lee, T. K.-M.; Zhu, N.; Yam, V. W.-W. *J. Am. Chem. Soc.* **2010**, *132*, 17646–17648. (h) Chen, Z.-H.; Zhang, L.-Y.; Chen, Z.-N. *Organometallics* **2012**, *31*, 256–260.

(4) (a) Crespo, O.; Gimeno, M. C.; Laguna, A.; Larraz, C.; Villacampa, M. D. *Chem.—Eur. J.* **2007**, *13*, 235–246. (b) Manbeck, G. F.; Brennessel, W. W.; Stockland, J.; Robert, A.; Eisenberg, R. *J. Am. Chem. Soc.* **2010**, *132*, 12307–12318. (c) Koshevoy, I. O.; Lin, C.-L.; Karttunen, A. J.; Jänis, J.; Haukka, M.; Tunik, S. P.; Chou, P.-T.; Pakkanen, T. A. *Inorg. Chem.* **2011**, *50*, 2395–2403. (d) Koshevoy, I. O.; Lin, C.-L.; Karttunen, A. J.; Jänis, J.; Haukka, M.; Tunik, S. P.; Chou, P.-T.; Pakkanen, T. A. *Chem.—Eur. J.* **2011**, *17*, 11456–11466.

(5) (a) Lu, W.; Zhu, N.; Che, C.-M. *J. Am. Chem. Soc.* **2003**, *125*, 16081−16088. (b) Koshevoy, I. O.; Lin, Y.-C.; Karttunen, A. J.; Chou, P.-T.; Vainiotalo, P.; Tunik, S. P.; Haukka, M.; Pakkanen, T. A. *Inorg. Chem.* **2009**, *48*, 2094−2102. (c) Koshevoy, I. O.; Karttunen, A. J.; Tunik, S. P.; Jänis, J.; Haukka, M.; Melnikov, A. S.; Serdobintsev, P. Y.; Pakkanen, T. A. *Dalton Trans.* **2010**, *39*, 2676−2683. (d) He, X.; Zhu, N.; Yam, V. W.-W. *Dalton Trans.* **2011**, *40*, 9703−9710.
(6) (a) Wang, Q.-M.; Lee, Y.-A.; Crespo, O.; Deaton, J.; Tang, C.; Gysling, H. J.; Gimeno, M. C.; Larraz, C.; Villacampa, M. D.; Laguna, A.; Eisenberg, R. *J. Am. Chem. Soc.* **2004**, *126*, 9488−9489. (b) Blanco, M. C.; Camara, J.; Gimeno, M. C.; Jones, P. G.; Laguna, A.; Lopez-de-Luzuriaga, J. M.; Olmos, M. E.; Villacampa, M. D. *Organometallics* **2012**, *31*, 2597−2605. (c) Tong, G. S. M.; Kui, S. C. F.; Chao, H.-Y.; Zhu, N.; Che, C.-M. *Chem.—Eur. J.* **2009**, *15*, 10777−10789.
(7) (a) Yip, S.-K.; Chan, C.-L.; Lam, W. H.; Cheung, K.-K.; Yam, V. W.-W. *Photochem. Photobiol. Sci.* **2007**, *6*, 365−371. (b) Koshevoy, I. O.; Karttunen, A. J.; Tunik, S. P.; Haukka, M.; Selivanov, S. I.; Melnikov, A. S.; Serdobintsev, P. Y.; Pakkanen, T. A. *Organometallics* **2009**, *28*, 1369−1376. (c) Koshevoy, I. O.; Ostrova, P. V.; Karttunen, A. J.; Melnikov, A. S.; Khodorkovskiy, M. A.; Haukka, M.; Jänis, J.; Tunik, S. P.; Pakkanen, T. A. *Dalton Trans.* **2010**, *39*, 9022−9031.
(8) (a) Wei, Q.-H.; Zhang, L.-Y.; Yin, G.-Q.; Shi, L.-X.; Chen, Z.-N. *J. Am. Chem. Soc.* **2004**, *126*, 9940−9941. (b) de la Riva, H.; Nieuwhuyzen, M.; Fierro, C. M.; Raithby, P. R.; Male, L.; Lagunas, M. C. *Inorg. Chem.* **2006**, *45*, 1418−1420. (c) Koshevoy, I. O.; Karttunen, A. J.; Shakirova, J. R.; Melnikov, A. S.; Haukka, M.; Tunik, S. P.; Pakkanen, T. A. *Angew. Chem., Int. Ed.* **2010**, *49*, 8864−8866.
(9) Koshevoy, I. O.; Lin, Y.-C.; Chen, Y.-C.; Karttunen, A. J.; Haukka, M.; Chou, P.-T.; Tunik, S. P.; Pakkanen, T. A. *Chem. Commun.* **2010**, *46*, 1440−1442.
(10) Krytchankou, I. S.; Krupenya, D. V.; Gurzhiy, V. V.; Belyaev, A. A.; Karttunen, A. J.; Koshevoy, I. O.; Melnikov, A. S.; Tunik, S. P. *J. Organomet. Chem.* **2013**, *723*, 65−71.
(11) Coates, G. E.; Parkin, C. *J. Chem. Soc.* **1962**, 3220−3226.
(12) *APEX2—Software Suite for Crystallographic Programs*; Bruker AXS, Inc.: Madison, WI, 2009.
(13) Sheldrick, G. M. *Acta Crystallogr., Sect. A* **2008**, *A64*, 112−122.
(14) Farrugia, L. J. *J. Appl. Crystallogr.* **1999**, *32*, 837−838.
(15) Sheldrick, G. M. *SADABS-2008/1−Bruker AXS Area Detector Scaling and Absorption Correction*; Bruker AXS: Madison, WI, 2008.
(16) Spek, A. L. *PLATON, A Multipurpose Crystallographic Tool*; Utrecht University: Utrecht, The Netherlands, 2005.
(17) Nardelli, M. *J. Appl. Crystallogr.* **1999**, *32*, 563−571.
(18) Demas, J. N.; Crosby, G. A. *J. Phys. Chem.* **1971**, *75*, 991−1024.
(19) (a) Perdew, J. P.; Burke, K.; Ernzerhof, M. *Phys. Rev. Lett.* **1996**, *77*, 3865−3868. (b) Adamo, C.; Barone, V. *J. Chem. Phys.* **1999**, *110*, 6158−6170.
(20) Weigend, F.; Ahlrichs, R. *Phys. Chem. Chem. Phys.* **2005**, *7*, 3297−3305.
(21) Andrae, D.; Häussermann, U.; Dolg, M.; Stoll, H.; Preuß, H. *Theor. Chem. Acc.* **1990**, *77*, 123−141.
(22) Schäfer, A.; Horn, H.; Ahlrichs, R. *J. Chem. Phys.* **1992**, *97*, 2571−2577.
(23) (a) Furche, F.; Rappoport, D. Density Functional Methods for Excited States: Equilibrium Structure and Electronic Spectra. In *Computational Photochemistry*; Olivucci, M., Ed.; Elsevier: Amsterdam, 2005; pp 93−128. (b) Furche, F.; Ahlrichs, R. *J. Chem. Phys.* **2002**, *117*, 7433−7447. (c) van Wüllen, C. *J. Comput. Chem.* **2011**, *32*, 1195−1201.
(24) Ahlrichs, R.; Bär, M.; Häser, M.; Horn, H.; Kölmel, C. *Chem. Phys. Lett.* **1989**, *162*, 165−169.
(25) Shakirova, J. R.; Grachova, E. V.; Gurzhiy, V. V.; Koshevoy, I. O.; Melnikov, A. S.; Sizova, O. V.; Tunik, S. P.; Laguna, A. *Dalton Trans.* **2012**, *41*, 2941−2949.
(26) Koshevoy, I. O.; Lin, Y.-C.; Karttunen, A. J.; Haukka, M.; Chou, P.-T.; Tunik, S. P.; Pakkanen, T. A. *Chem. Commun.* **2009**, 2860−2862.
(27) Chou, P.-T.; Chi, Y.; Chung, M.-W.; Lin, C.-C. *Coord. Chem. Rev.* **2011**, *255*, 2653−2665.